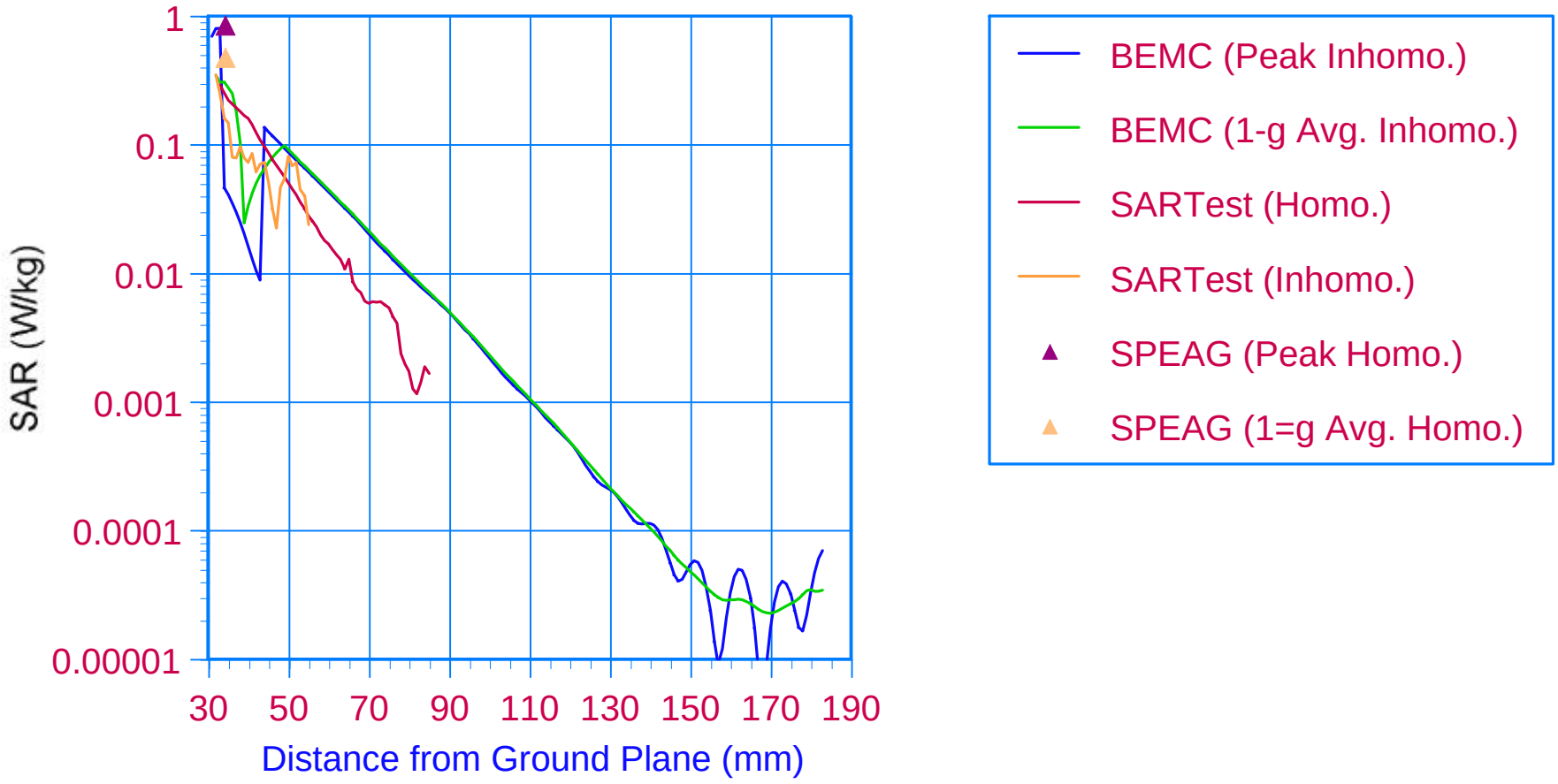

Figure 8.16. Comparison of maximum FDTD derived and measured SARs as a function of the perpendicular distance (31 to 190 mm) from ground plane in line with the center of the lower left patch causing highest SAR in slab models exposed to AT&T RU antenna.

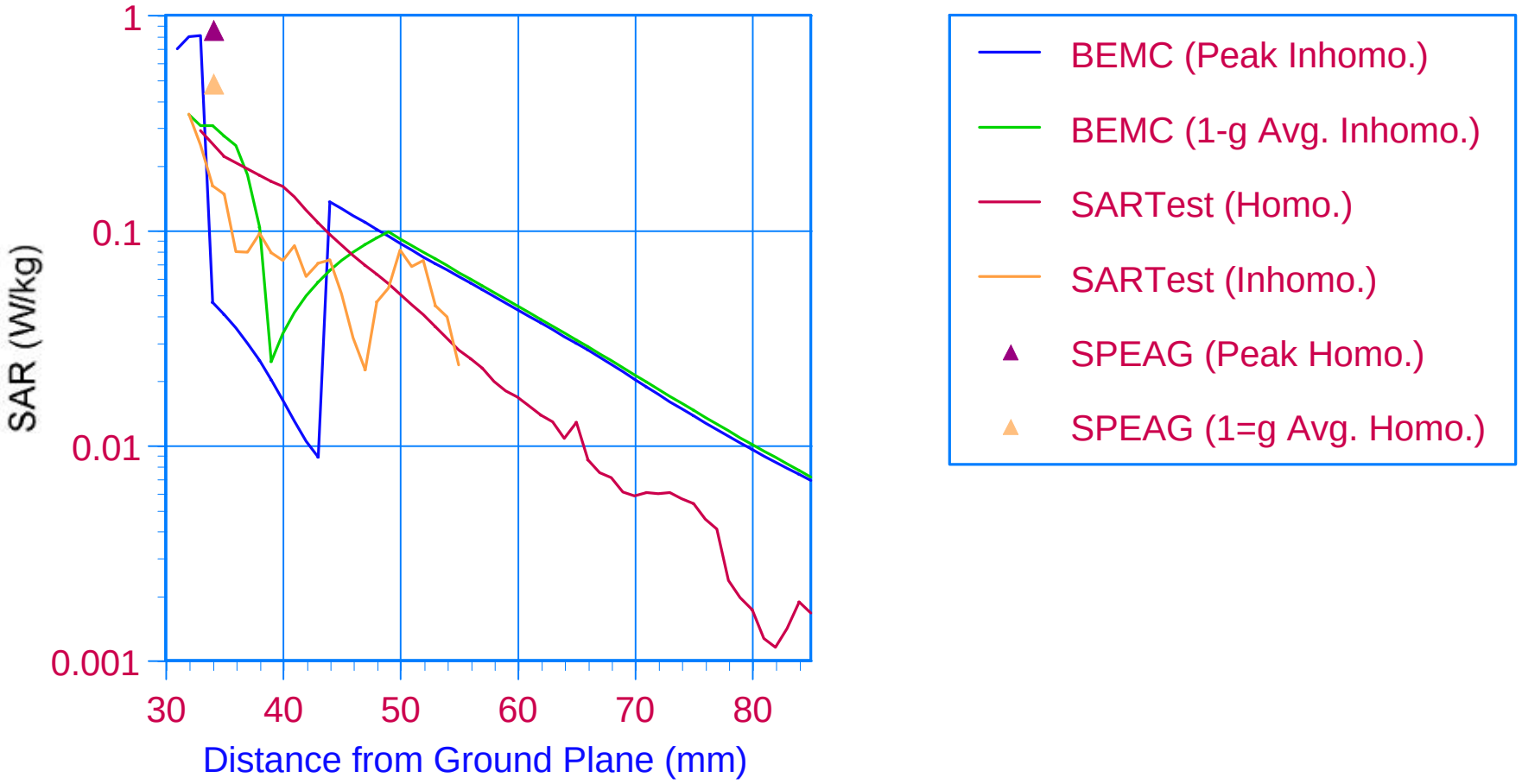

Figure 8.17. Comparison of maximum FDTD derived and measured SARs as a function of the perpendicular distance (31 to 80 mm) from ground plane in line with the center of the lower left patch causing highest SAR in slab models exposed to AT&T RU antenna.

8.2 Exposure to Single Feed Antenna

FDTD calculations of the SAR distributions in the inhomogeneous slab model were made for the case where the slab was exposed to the AT&T RTU antenna with 79.62 mW fed to the lower feed with the second upper feed terminated with a 50-ohm load. Comparison of the calculated SAR and 1 gram average SAR distributions were made with the corresponding distributions calculated for the double feed antenna discussed in the above section.

Figure 8.18 illustrates a comparison of the SAR distributions over the yz plane in the skin layer of the slab inhomogeneous model exposed to the 2 feed model (left side of figure) and the 1 feed model (right side of figure). The plane corresponded to the location at x=50 mm (34 mm from the groundplane) next to the scan denoted by E in Figures 3.8 and 3.9. This layer was chosen for comparison of results obtained with the different feed configurations since it provides a good map of the near fields and the associated SAR distributions allowing easy identification of locations of maximum SAR. The maximum calculated SAR for the entire model was easily identified as 0.849 W/kg at the location in the skin near the center of the upper left patch (denoted by a + sign). The corresponding calculated SAR in this layer for the model exposed to the double feed antenna was 0.790 W/kg occurring in the skin near the center of the lower right patch (denoted by a + sign). The maximum SAR of 0.805 W/kg for the entire model for the latter exposure conditions occurred in the adjacent plane at x=49 mm. Overall the SAR distributions appear nearly identical with a maximum SAR difference of only 0.23 dB. The significant drop in the SAR near the upper feed position and the increase in SAR near the lower feed position for exposure of the model to the single feed antenna is as expected but there is little change in the fields near the patches which are most responsible for establishing the patterns of the maximum SAR produced by the antenna.

Figure 8.19 compares the SAR distributions in the yz plane at x=56 mm in the fat layer of the model denoted by scan F in Figures 3.8 and 3.9. Here the maximum SARs have dropped significantly due to the lower conductivity of the fat layer with only a 0.06 dB difference between the respective 0.0213 W/kg and 0.0216 W/kg obtained for exposure of the model to the 2 feed and 1 feed antenna configurations. Figure 8.20 compares the SAR distributions in the yz plane at x=62 mm in the muscle layer denoted by scan G in Figures 3.8 and 3.9. With the higher conductivity of the muscle tissue, the maximum SARs have increased to 0.125 W/kg and 0.130 W/kg, respectively for exposure of the model to the 2 feed and 1 feed antenna configurations, corresponding to a difference of 0.17 dB.

Figure 8.21 compares the 1 gram average SAR distributions in the xz planes through the center of the left column of patches at y=81 mm (scan O, Figure 3.9), through the center of the patch array at y=154 mm (scan P, Figure 3.9) and through the center of the right column of patches at y=228 mm (scan Q, Figure 3.9) exposed to the 2 feed and 1

feed antennas. The maximum 1-gram average calculated SAR for exposure of the model to the 2 feed antenna was 0.338 W/kg (6.75 dB below the FCC MPL) occurring adjacent to the lower left patch. The corresponding 1-gram average SAR for exposure of the model to the 1 feed antenna was 0.363 W/kg (6.44 dB below the FCC MPL) occurring adjacent to the upper left patch.

Since the highest SAR occurred in the tissue of the model in front of the patches of the antenna array, a plot was made to compare the calculated SARs in a line perpendicular to the ground plane and through the center of the patch producing the fields that caused the highest SAR. Figure 8.22 illustrates the plot where the blue line denotes the SAR calculated for the model exposed to the 2 feed antenna and the red line denotes the SAR calculated for the model exposed to the single feed antenna. We can conclude from these results that there is insignificant difference in the FDTD derived SAR distributions in the model when exposed to either the 2 feed or the 1 feed antenna configurations with the same total input power.

SPEAG conducted measurements of peak, 1 gram average and 10 gram average SAR in a homogeneous slab model as discussed in pages 25 through 28 of Appendix A and in Appendix G of Appendix A. The measurements were based on a Fiberglas box filled with liquid having a relative permittivity of 40.9 and conductivity of 1.83 similar to that they used for the Kuster head model measurements. The measurements were made with the 4-mm thick Fiberglas bottom of the liquid filled container placed at various distances from the antenna. At the closest distance the Fiberglas bottom was in contact with the radome so the bottom surface of the liquid was 4-mm from the radome. The measurements were made with the probe in the liquid and 4-mm above the bottom surface of the liquid. Only the measurements with the model in contact with the radome are comparable to the FDTD derived values since the slab model computer calculations were made with the models in contact with the radome. The maximum measured peak and 1 gram average SAR were 0.860 W/kg and 0.484 W/kg respectively for the homogeneous slab phantom as compared to the respective calculated values of 0.805 W/kg and 0.346 W/kg for the inhomogeneous slab model. Since the homogeneous model had a higher conductivity than the muscle tissue in the inhomogeneous slab model and is reported to represent the worst case of maximum-coupled power and SAR, the higher measured SAR values for the former look very reasonable.

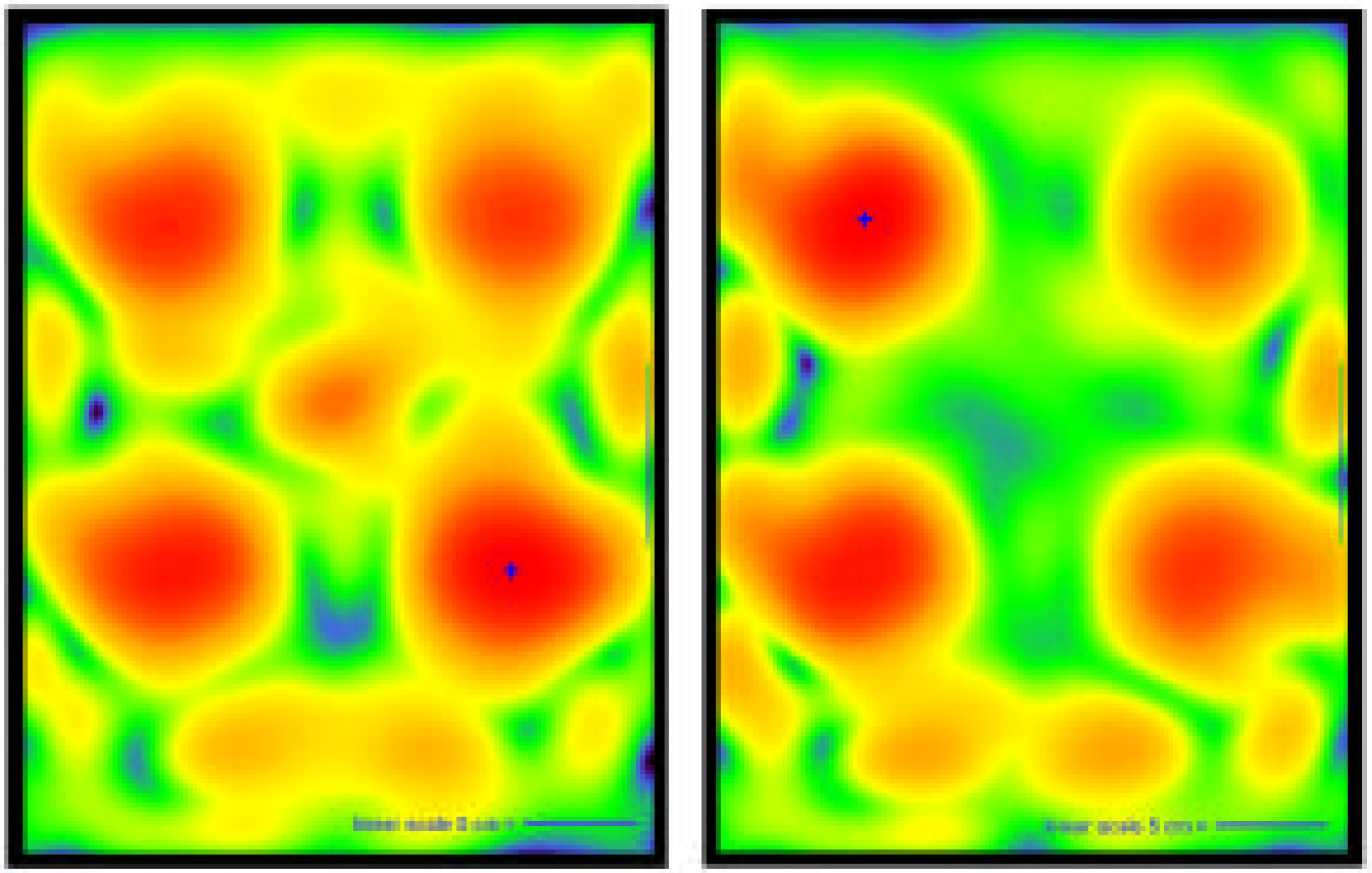

Figure 8.18. Comparison of calculated SAR distribution in yz plane at x=50 mm in skin layer of inhomogeneous slab model exposed to AT&T RU antenna with 1 feed and 2 feeds (+ denotes location of maximum SAR in yz plane).

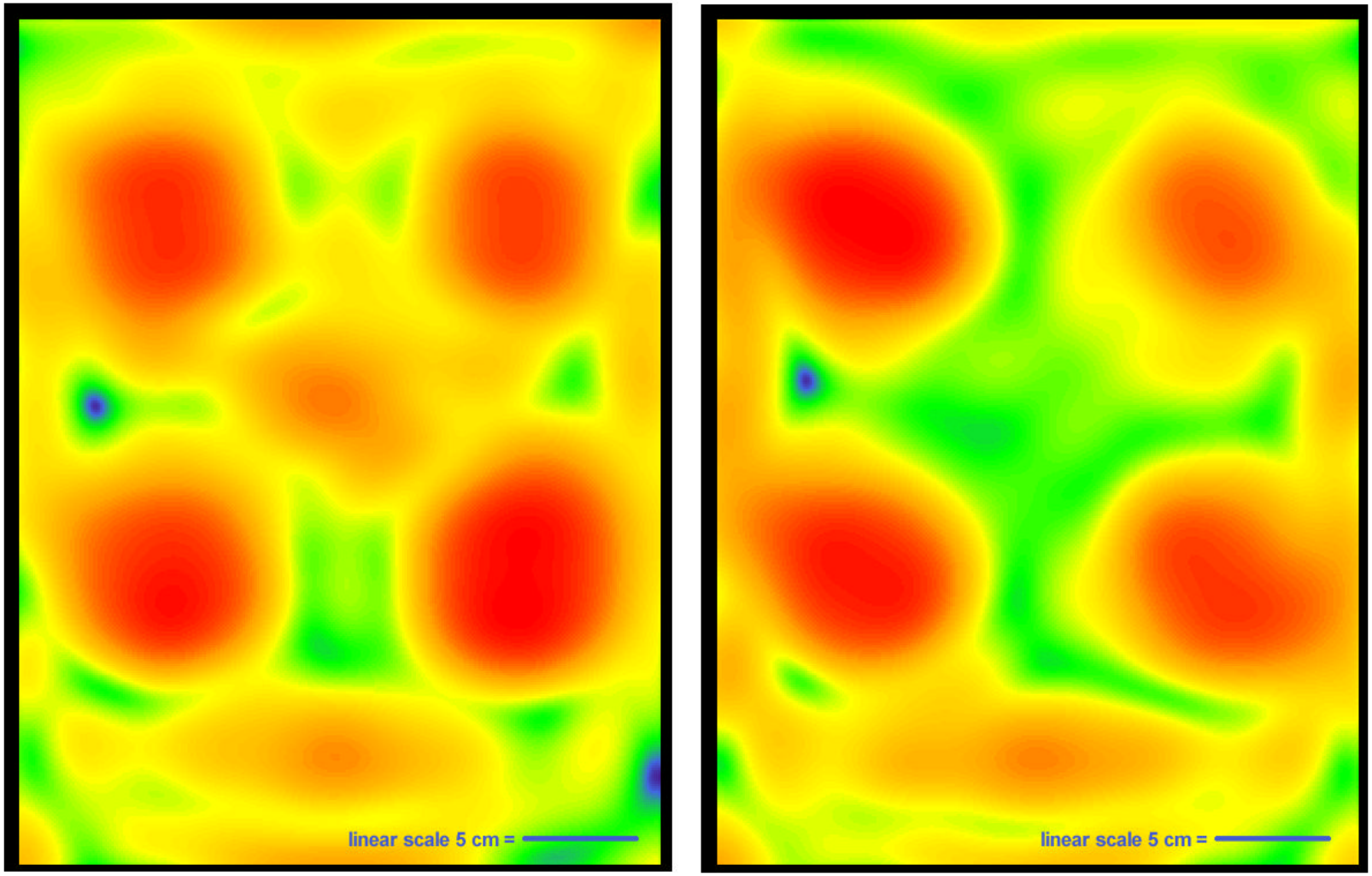

2 feeds 0 dB = 0.0213 W/kg

1 feed 0 dB = 0.0216 W/kg

Figure 8.19. Comparison of calculated SAR distribution in yz plane at x=56 mm in fat layer of inhomogeneous slab model exposed to AT&T RU antenna with 1 feed and 2 feeds.

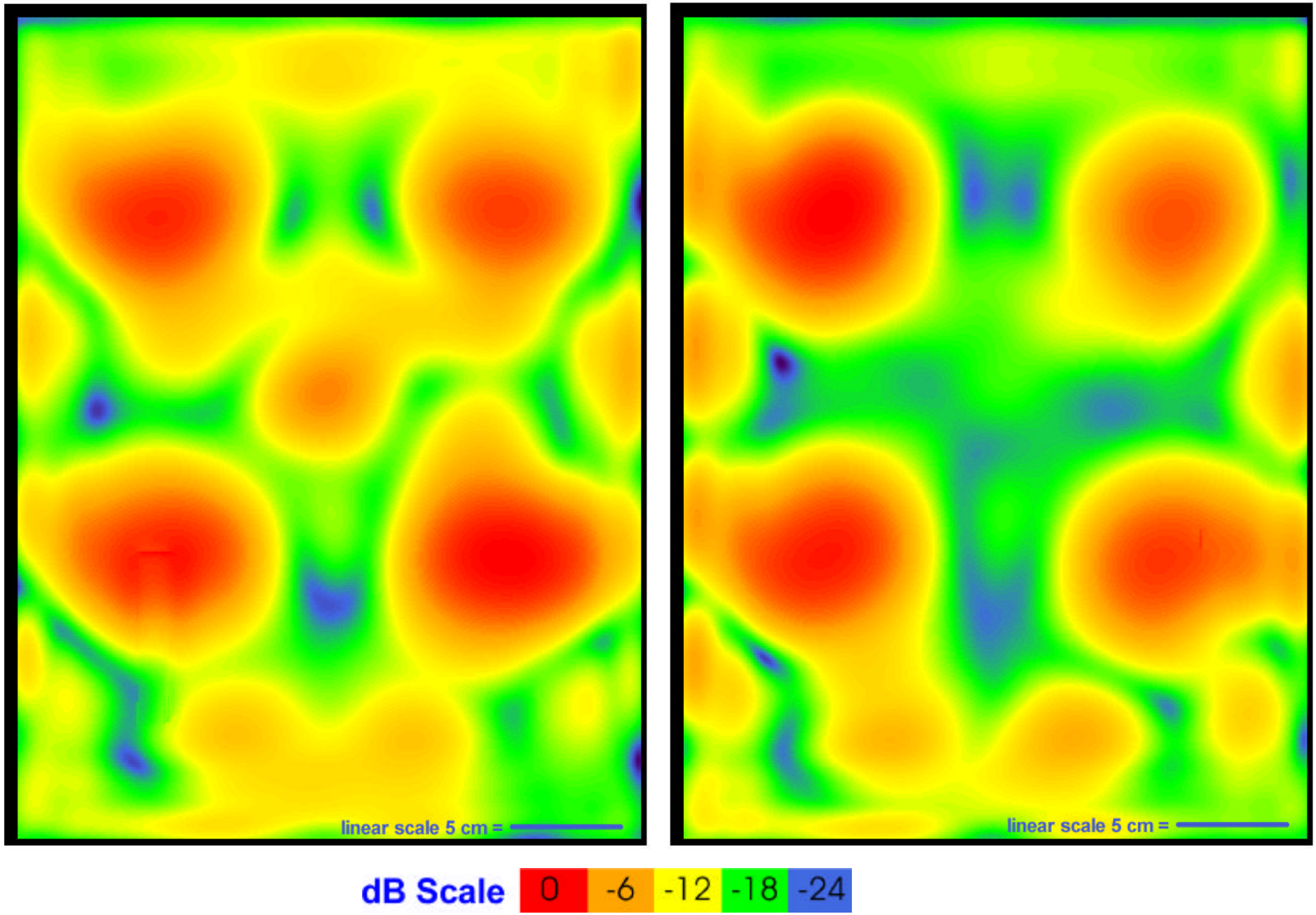

2 feeds 0 dB = 0.125 W/kg

1 feed 0 dB = 0.130 W/kg

Figure 8.20. Comparison of calculated SAR distribution in yz plane at x=62 mm in muscle layer of inhomogeneous slab model exposed to AT&T RU antenna with 1 feed and 2 feeds.

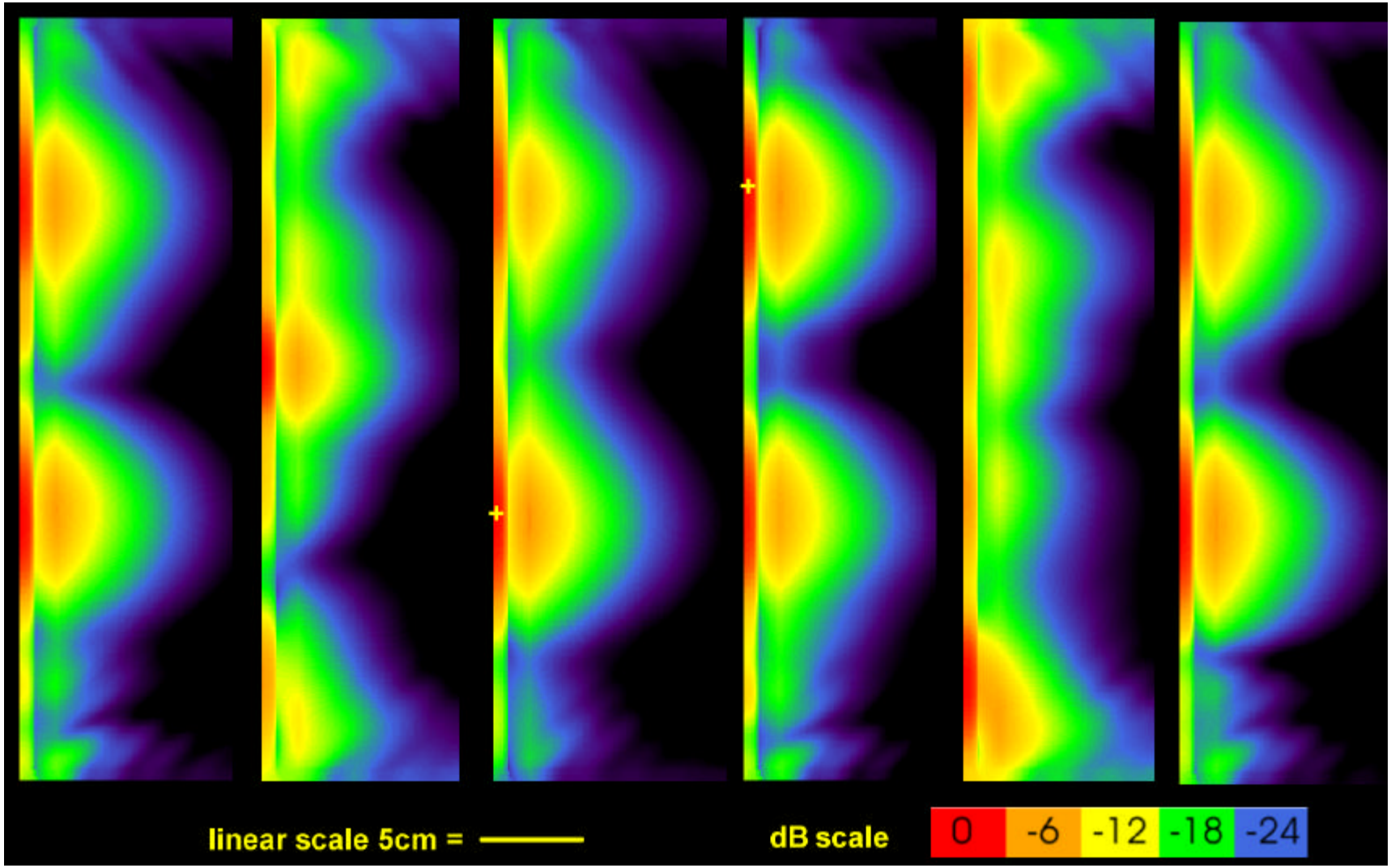

----------2 feeds---------- ----------1 feed----------

Scan O, y=81	P, y=154	Q, y=228	O, y=81	P, y=154	Q, y=228 mm
Max SAR=0.275	0.128	0.338	0.363	0.317	0.231 W/kg

Figure 8.21. Comparison of calculated 1 gram average SAR distribution in xz planes through center of patches and patch array in inhomogeneous slab model exposed to AT&T RU antenna with 1 feed and 2 feeds (+ signs denote maximum SAR for each scan group).

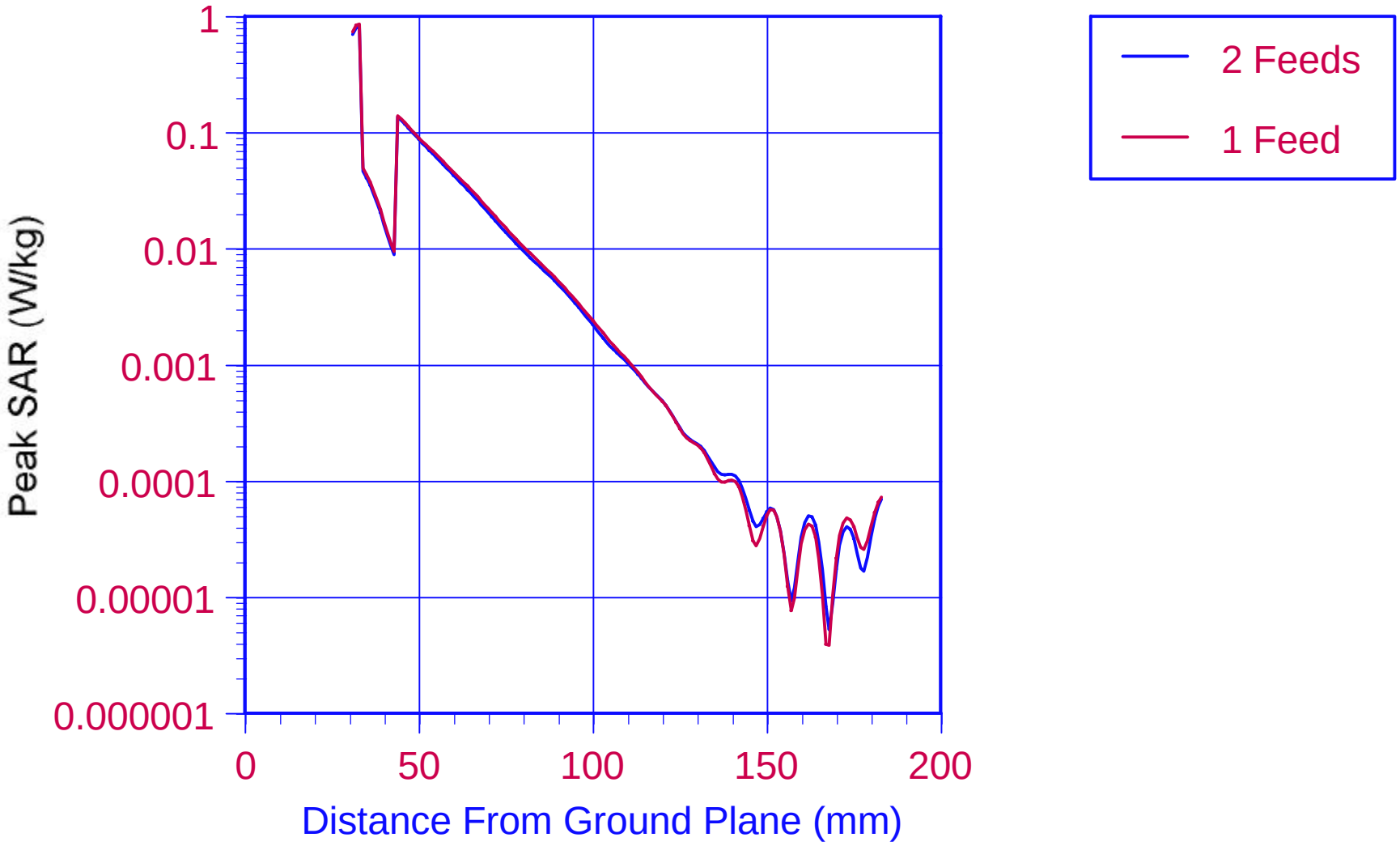

Figure 8.22. Comparison of maximum FDTD derived SARs as a function of perpendicular distance from ground plane in line with center of patch causing highest SAR in inhomogeneous slab model exposed to AT&T RU antenna with 2 feeds and 1 feed.

9 FDTD Calculation of SAR in Homogeneous Rectangular Slab Torso Model

In order to better compare the FDTD calculations of the SAR distributions with the measured values for exposed slab tissue models a homogeneous slab model equivalent to that used by SPEAG was introduced into the FDTD program. The configuration of the model was the same as that shown in Figures 3.8 and 3.9 except the skin and fat layers of the homogeneous model were replaced by a 4-mm thick Fiberglas layer separating the muscle tissue layer from the radome. The dielectric properties of the muscle were set to correspond to the values of the liquid used by SPEAG for their measurements. Figure 9.1 illustrates the calculated SAR distribution in xz planes through the slab model corresponding to the vertical slices O (through the center of the left row of antenna patches), P (through the center of the array of patches) and Q (through the right row of patches) defined in Figure 3.9. The maximum SAR was found to be 0.890 W/kg in the muscle medium in front of the lower right patch of the antenna. Figure 9.2 illustrates the calculated SAR distribution in the yz plane (1-mm from the surface of the liquid, 5-mm from the radome, 35-mm from the ground plane and 53-mm from the coordinate system origin) where the black + sign indicates the position of maximum SAR. Figure 9.3 illustrates the calculated SAR distribution in the in the yz plane at 4-mm from the surface of the liquid or 39-mm from the ground plane, the same location where the measurements were conducted. The maximum SAR for this plane was 0.645 W/kg in contrast with the maximum probe measurement of 0.860 W/kg. Since the spatial resolution of the FDTD derived SAR is 1-mm and that of the probe is somewhat larger due to the finite size of its sensing dipoles the probe may be measuring a higher value of SAR due to the influence of the higher surface SAR. The gradient of the SAR is very high near the surface of the slab phantom. The calculated SAR distributions compare very favorably with the measured values displayed in Appendix A.

Figure 9.4 illustrates the calculated 1-gram average SAR distribution in the yz plane at 1-mm from the surface of the liquid or 35-mm from the ground plane. The maximum value was found to be 0.584 W/kg. Figure 9.5 illustrates the 1 gram average SAR distribution in the yz plane at 4-mm from the surface of the liquid or 39-mm from the ground plane were the measurements were conducted. The maximum value was found to be 0.534 W/kg as compared to the measured value of 0.484 W/kg.

Table 9.1 illustrates the results of the 1-gram averaging of the FDTD output data for the homogeneous slab model, which can be related to the FCC MPL. It may be noted from the table that the highest 1-g average SAR for the entire model is 0.5958 W/kg occurring at x = 52-mm, y = 229-mm and z = 141-mm. This is 4.3 dB below FCC MPL of 1.6 W/kg. Using the same procedure as outlined in the previous section for the inhomogeneous slab model, the total absorbed power is calculated to be 74.18 mW, which is 93.2% of the antenna, input power. Thus the whole-body averaged SAR for an

adult man with a torso similar to that of the homogeneous slab model would be somewhere between 0.001377 and 0.004893 W/kg or from 16 to 58 times less than that allowed by the FCC MPL of 0.08 W/kg.

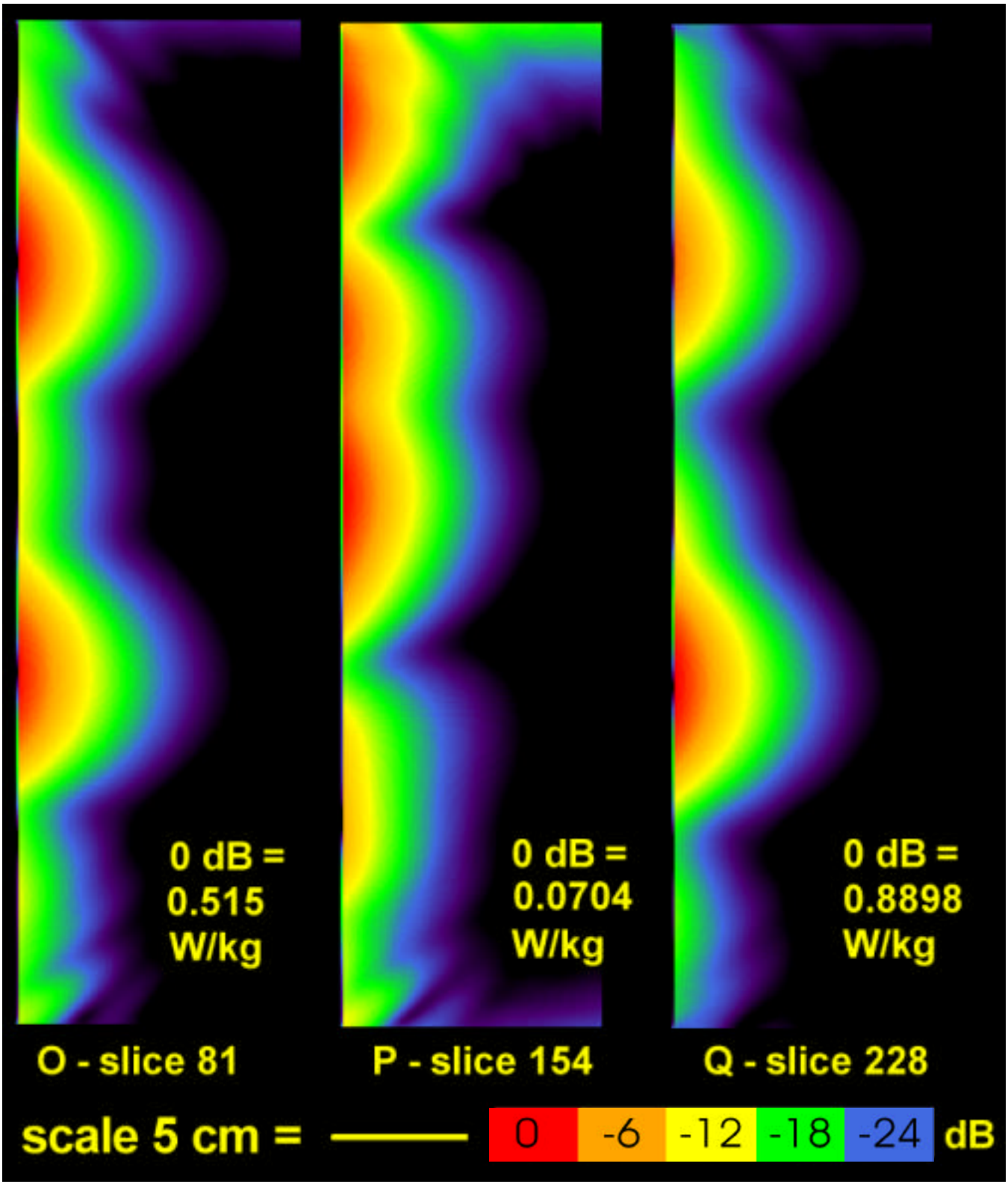

Figure 9.1. FDTD derived x-z plane SAR distributions in homogeneous slab model exposed to AT&T RU antenna.

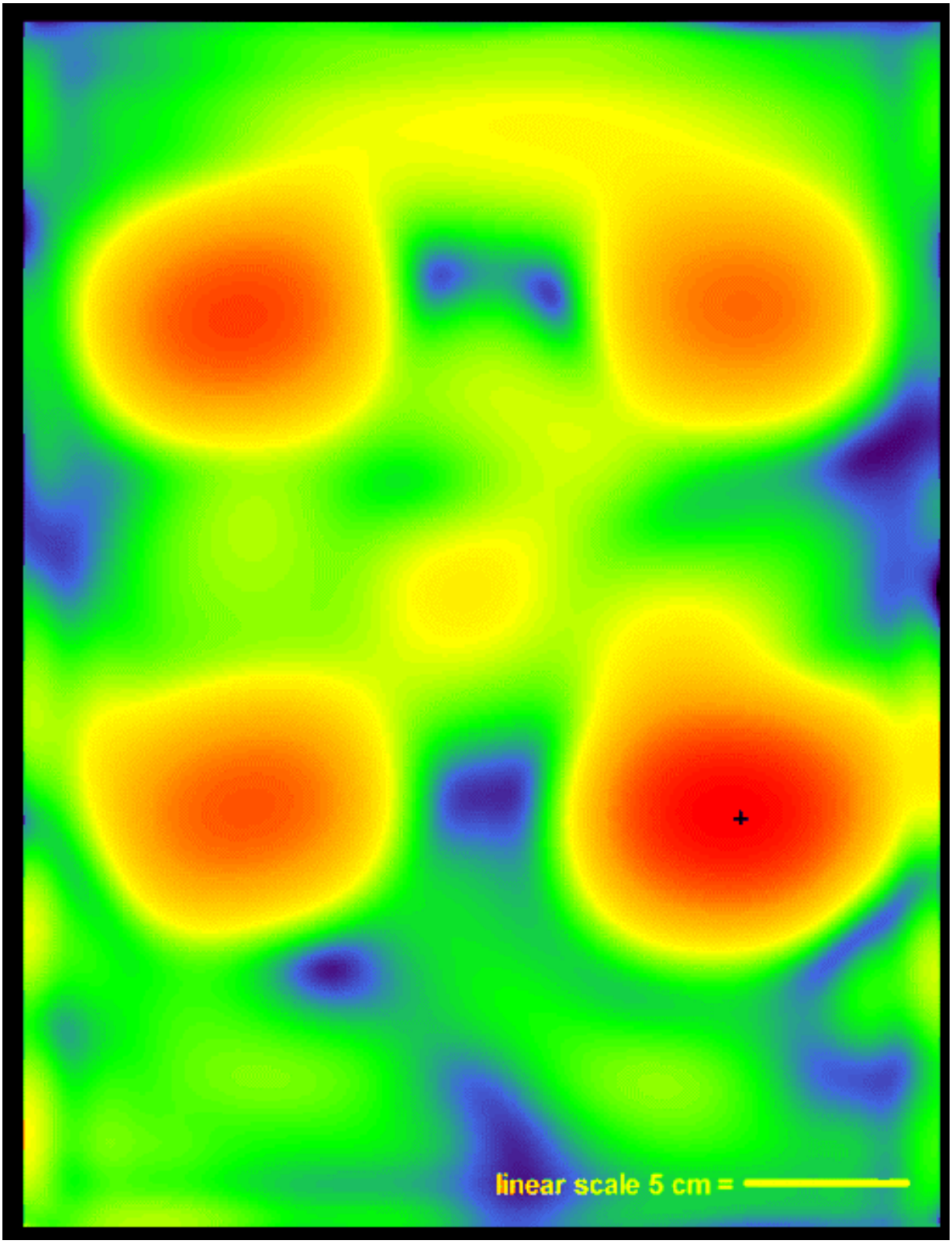

Scale 0 dB = 0.890 W/kg

Figure 9.2. FDTD derived y-z plane SAR distribution at surface of liquid in homogeneous slab model exposed to AT&T RU antenna (+ sign indicates position of maximum SAR.

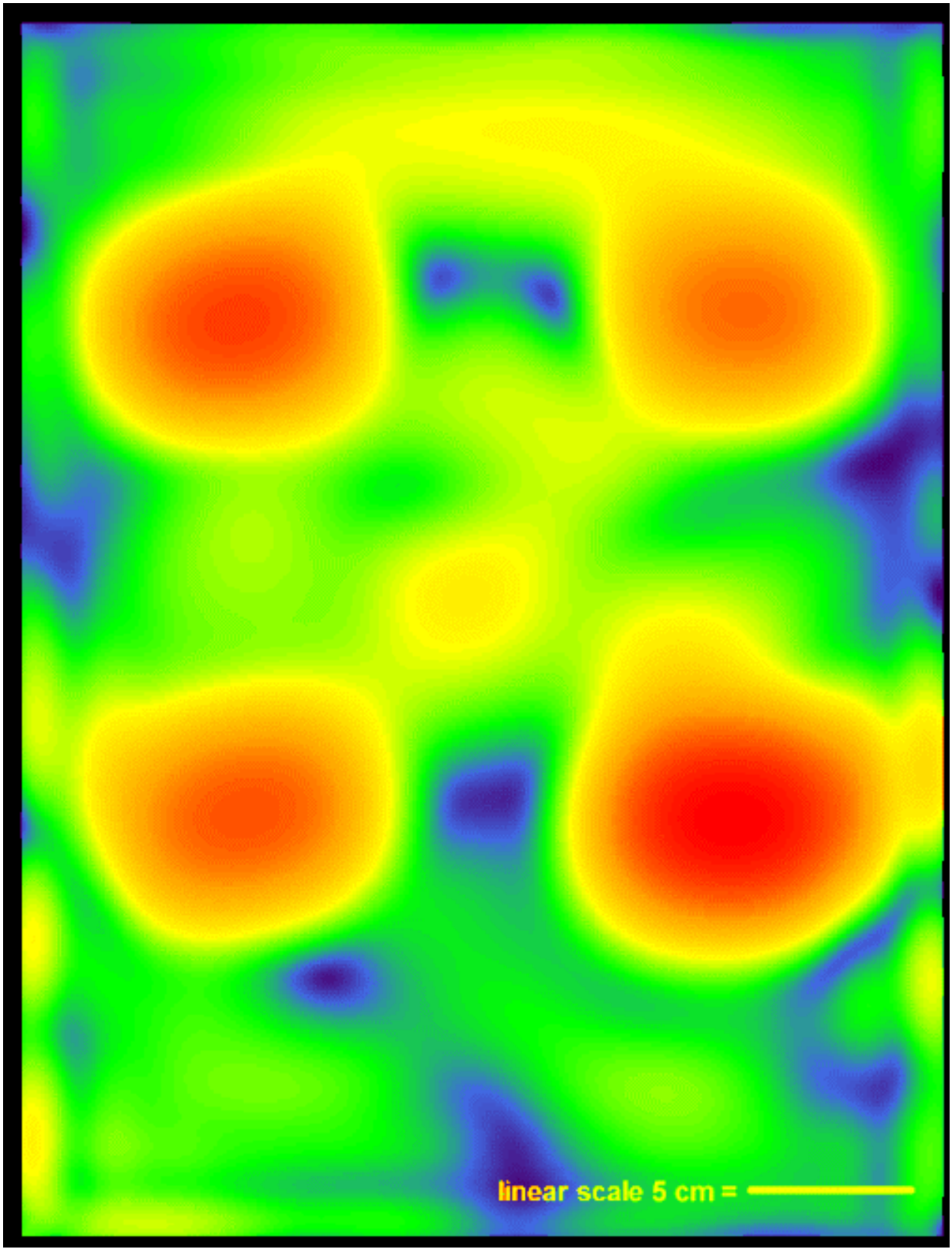

Figure 9.3. FDTD derived y-z plane SAR distribution at 4mm from surface of liquid in homogeneous slab model exposed to AT&T RU antenna.

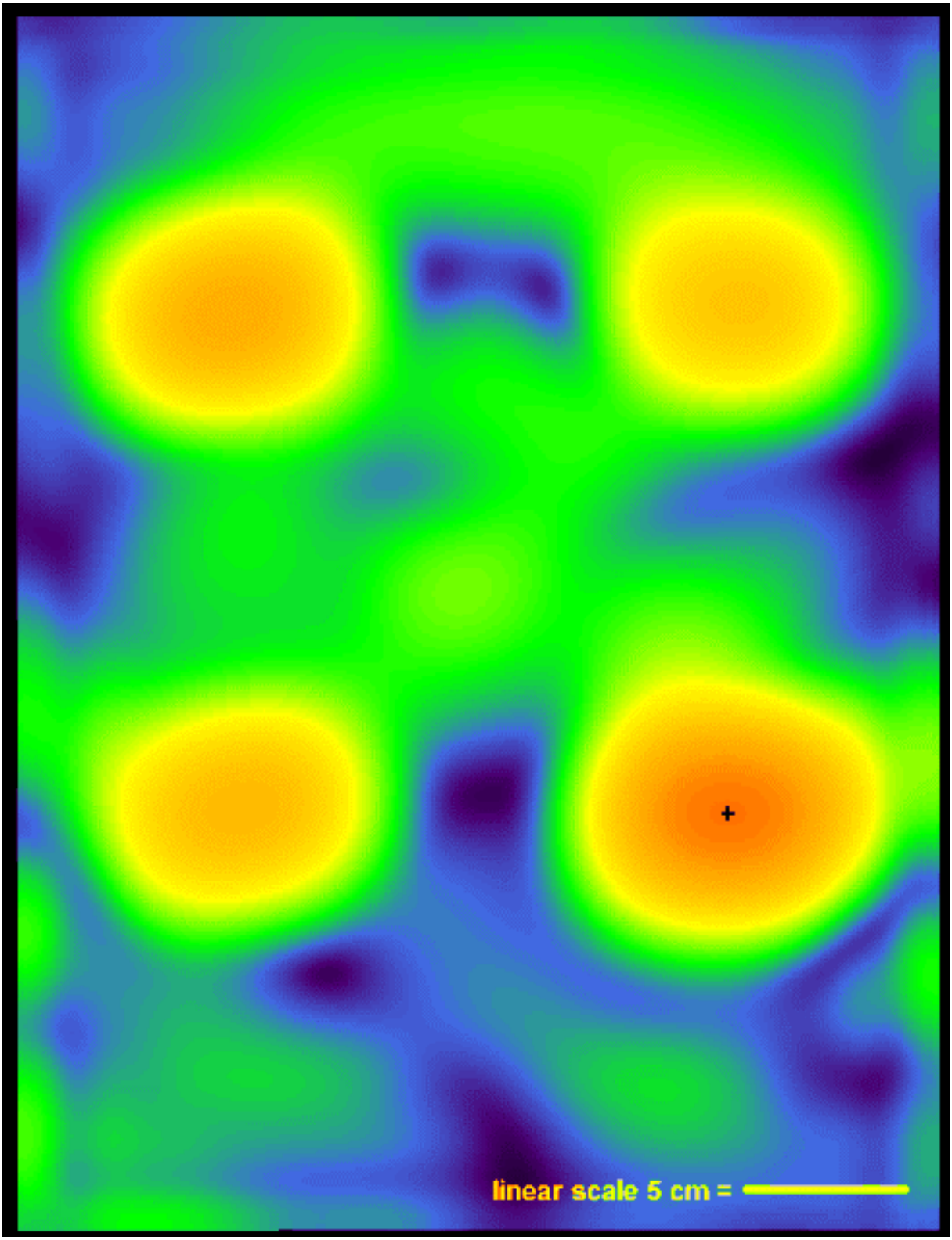

Scale 0 dB = 0.584 W/kg

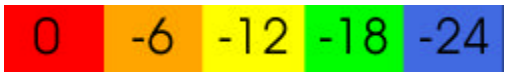

Figure 9.4. FDTD derived y-z plane 1 gram average SAR distribution at surface of liquid in homogeneous slab model exposed to AT&T RU antenna (+ sign indicates position of maximum SAR.

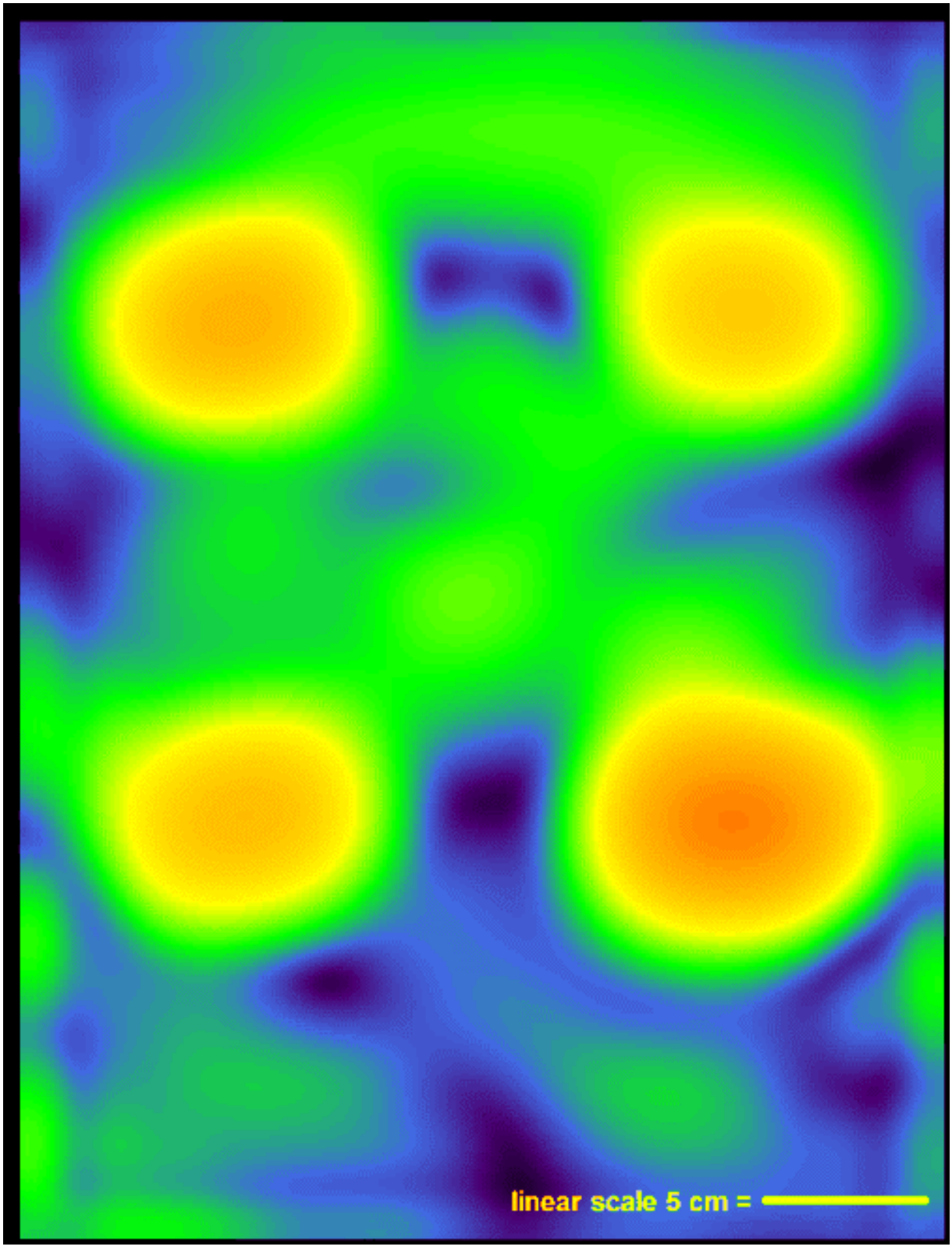

Figure 9.5. FDTD derived y-z plane 1 gram average SAR distribution at 4 mm above surface of liquid in homogeneous slab model exposed to AT&T RU antenna.

Table 9.1. Slice and Whole Slab Model Peak and average (averaged over slice) 1 Gram Average SAR for Homogeneous Slab Model Exposed to AT&T RU Antenna with Outside Skin Surface in Contact with Radome Centered at Middle of Patch Array (xz-plane slice file number is distance in mm from FDTD space rectangular coordinates origin in x direction).

Name of Slice Data File	Peak SAR y and z coordinates		Peak SAR (W/kg)	Avg. SAR (W/kg)	Voxels in tissue
kusslb.yz52.1gsar	229	141	0.5958E+00	0.5042E-01	101748
kusslb.yz53.1gsar	229	141	0.5844E+00	0.4948E-01	101748
kusslb.yz54.1gsar	229	141	0.5691E+00	0.4824E-01	101748
kusslb.yz55.1gsar	229	141	0.5520E+00	0.4684E-01	101748
kusslb.yz56.1gsar	229	141	0.5341E+00	0.4537E-01	101748
kusslb.yz57.1gsar	229	141	0.5677E+00	0.4808E-01	101748
kusslb.yz58.1gsar	229	141	0.5102E+00	0.4338E-01	101748
kusslb.yz59.1gsar	229	141	0.4586E+00	0.3915E-01	101748
kusslb.yz60.1gsar	229	141	0.4124E+00	0.3530E-01	101748
kusslb.yz61.1gsar	229	141	0.3708E+00	0.3182E-01	101748
kusslb.yz62.1gsar	229	141	0.3334E+00	0.2867E-01	101748
kusslb.yz63.1gsar	229	141	0.2998E+00	0.2581E-01	101748
kusslb.yz64.1gsar	229	141	0.2696E+00	0.2324E-01	101748
kusslb.yz65.1gsar	229	141	0.2424E+00	0.2091E-01	101748
kusslb.yz66.1gsar	229	141	0.2180E+00	0.1881E-01	101748
kusslb.yz67.1gsar	229	141	0.1960E+00	0.1692E-01	101748
kusslb.yz68.1gsar	229	141	0.1762E+00	0.1523E-01	101748
kusslb.yz69.1gsar	229	141	0.1583E+00	0.1370E-01	101748
kusslb.yz70.1gsar	229	141	0.1423E+00	0.1233E-01	101748
kusslb.yz71.1gsar	228	141	0.1280E+00	0.1109E-01	101748
kusslb.yz72.1gsar	228	141	0.1151E+00	0.9975E-02	101748
kusslb.yz73.1gsar	228	141	0.1034E+00	0.8967E-02	101748
kusslb.yz74.1gsar	228	141	0.9299E-01	0.8057E-02	101748
kusslb.yz75.1gsar	228	141	0.8357E-01	0.7237E-02	101748
kusslb.yz76.1gsar	228	141	0.7509E-01	0.6499E-02	101748
kusslb.yz77.1gsar	228	141	0.6745E-01	0.5836E-02	101748
kusslb.yz78.1gsar	228	141	0.6057E-01	0.5241E-02	101748
kusslb.yz79.1gsar	227	141	0.5437E-01	0.4710E-02	101748
kusslb.yz80.1gsar	227	141	0.4880E-01	0.4234E-02	101748
kusslb.yz81.1gsar	227	141	0.4379E-01	0.3809E-02	101748
kusslb.yz82.1gsar	227	141	0.3930E-01	0.3428E-02	101748
kusslb.yz83.1gsar	227	141	0.3526E-01	0.3086E-02	101748
kusslb.yz84.1gsar	228	141	0.3166E-01	0.2779E-02	101748
kusslb.yz85.1gsar	228	141	0.2843E-01	0.2504E-02	101748
kusslb.yz86.1gsar	228	141	0.2553E-01	0.2256E-02	101748
kusslb.yz87.1gsar	229	141	0.2294E-01	0.2033E-02	101748
kusslb.yz88.1gsar	229	141	0.2063E-01	0.1833E-02	101748
kusslb.yz89.1gsar	230	141	0.1855E-01	0.1653E-02	101748
kusslb.yz90.1gsar	230	141	0.1669E-01	0.1492E-02	101748
kusslb.yz91.1gsar	230	141	0.1502E-01	0.1347E-02	101748
kusslb.yz92.1gsar	230	141	0.1351E-01	0.1218E-02	101748
kusslb.yz93.1gsar	231	141	0.1216E-01	0.1101E-02	101748
kusslb.yz94.1gsar	231	141	0.1094E-01	0.9959E-03	101748
kusslb.yz95.1gsar	230	141	0.9849E-02	0.9013E-03	101748
kusslb.yz96.1gsar	230	141	0.8864E-02	0.8158E-03	101748
kusslb.yz97.1gsar	230	141	0.7977E-02	0.7387E-03	101748
kusslb.yz98.1gsar	230	141	0.7178E-02	0.6690E-03	101748
kusslb.yz99.1gsar	230	141	0.6455E-02	0.6060E-03	101748

Name of Slice Data File	Peak SAR y and z coordinates		Peak SAR (W/kg)	Avg. SAR (W/kg)	Voxels in tissue
kusslb.yz100.1gsa	230	141	0.5802E-02	0.5492E-03	101748
kusslb.yz101.1gsa	229	141	0.5213E-02	0.4980E-03	101748
kusslb.yz102.1gsa	229	141	0.4680E-02	0.4518E-03	101748
kusslb.yz103.1gsa	15	16	0.4384E-02	0.4103E-03	101748
kusslb.yz104.1gsa	15	16	0.4255E-02	0.3728E-03	101748
kusslb.yz105.1gsa	15	16	0.4125E-02	0.3391E-03	101748
kusslb.yz106.1gsa	15	16	0.3996E-02	0.3088E-03	101748
kusslb.yz107.1gsa	15	16	0.3870E-02	0.2815E-03	101748
kusslb.yz108.1gsa	15	16	0.3749E-02	0.2569E-03	101748
kusslb.yz109.1gsa	15	16	0.3633E-02	0.2349E-03	101748
kusslb.yz110.1gsa	15	16	0.3522E-02	0.2150E-03	101748
kusslb.yz111.1gsa	15	16	0.3419E-02	0.1972E-03	101748
kusslb.yz112.1gsa	15	16	0.3322E-02	0.1813E-03	101748
kusslb.yz113.1gsa	15	16	0.3232E-02	0.1669E-03	101748
kusslb.yz114.1gsa	15	16	0.3149E-02	0.1540E-03	101748
kusslb.yz115.1gsa	15	16	0.3071E-02	0.1425E-03	101748
kusslb.yz116.1gsa	15	16	0.2999E-02	0.1320E-03	101748
kusslb.yz117.1gsa	15	16	0.2932E-02	0.1226E-03	101748
kusslb.yz118.1gsa	15	16	0.2870E-02	0.1142E-03	101748
kusslb.yz119.1gsa	15	16	0.2811E-02	0.1066E-03	101748
kusslb.yz120.1gsa	15	16	0.2755E-02	0.9977E-04	101748
kusslb.yz121.1gsa	15	16	0.2703E-02	0.9365E-04	101748
kusslb.yz122.1gsa	15	16	0.2652E-02	0.8817E-04	101748
kusslb.yz123.1gsa	15	16	0.2604E-02	0.8324E-04	101748
kusslb.yz124.1gsa	15	16	0.2558E-02	0.7881E-04	101748
kusslb.yz125.1gsa	15	16	0.2514E-02	0.7480E-04	101748
kusslb.yz126.1gsa	15	16	0.2472E-02	0.7119E-04	101748
kusslb.yz127.1gsa	15	16	0.2431E-02	0.6791E-04	101748
kusslb.yz128.1gsa	15	16	0.2392E-02	0.6494E-04	101748
kusslb.yz129.1gsa	15	16	0.2356E-02	0.6226E-04	101748
kusslb.yz130.1gsa	15	16	0.2321E-02	0.5986E-04	101748
kusslb.yz131.1gsa	15	16	0.2289E-02	0.5773E-04	101748
kusslb.yz132.1gsa	15	16	0.2260E-02	0.5585E-04	101748
kusslb.yz133.1gsa	15	16	0.2233E-02	0.5421E-04	101748
kusslb.yz134.1gsa	15	16	0.2208E-02	0.5278E-04	101748
kusslb.yz135.1gsa	15	16	0.2187E-02	0.5154E-04	101748
kusslb.yz136.1gsa	15	16	0.2168E-02	0.5047E-04	101748
kusslb.yz137.1gsa	15	16	0.2152E-02	0.4953E-04	101748
kusslb.yz138.1gsa	15	16	0.2139E-02	0.4871E-04	101748
kusslb.yz139.1gsa	15	16	0.2129E-02	0.4800E-04	101748
kusslb.yz140.1gsa	15	16	0.2121E-02	0.4740E-04	101748
kusslb.yz141.1gsa	15	16	0.2116E-02	0.4689E-04	101748
kusslb.yz142.1gsa	15	16	0.2113E-02	0.4650E-04	101748
kusslb.yz143.1gsa	15	16	0.2112E-02	0.4621E-04	101748
kusslb.yz144.1gsa	15	16	0.2113E-02	0.4602E-04	101748
kusslb.yz145.1gsa	15	16	0.2116E-02	0.4593E-04	101748
kusslb.yz146.1gsa	15	16	0.2120E-02	0.4592E-04	101748
kusslb.yz147.1gsa	15	16	0.2125E-02	0.4598E-04	101748
kusslb.yz148.1gsa	15	16	0.2130E-02	0.4607E-04	101748
kusslb.yz149.1gsa	15	16	0.2135E-02	0.4619E-04	101748
kusslb.yz150.1gsa	15	16	0.2141E-02	0.4631E-04	101748
kusslb.yz151.1gsa	15	16	0.2146E-02	0.4644E-04	101748
kusslb.yz152.1gsa	15	16	0.2150E-02	0.4657E-04	101748
kusslb.yz153.1gsa	15	16	0.2153E-02	0.4671E-04	101748
kusslb.yz154.1gsa	15	16	0.2155E-02	0.4687E-04	101748

Name of Slice Data File	Peak SAR y and z coordinates		Peak SAR (W/kg)	Avg. SAR (W/kg)	Voxels in tissue
kusslb.yz155.1gsa	15	16	0.2156E-02	0.4706E-04	101748
kusslb.yz156.1gsa	15	16	0.2155E-02	0.4729E-04	101748
kusslb.yz157.1gsa	15	16	0.2152E-02	0.4756E-04	101748
kusslb.yz158.1gsa	15	16	0.2148E-02	0.4785E-04	101748
kusslb.yz159.1gsa	15	16	0.2142E-02	0.4817E-04	101748
kusslb.yz160.1gsa	15	16	0.2134E-02	0.4849E-04	101748
kusslb.yz161.1gsa	15	16	0.2125E-02	0.4880E-04	101748
kusslb.yz162.1gsa	15	16	0.2114E-02	0.4909E-04	101748
kusslb.yz163.1gsa	15	16	0.2101E-02	0.4936E-04	101748
kusslb.yz164.1gsa	15	16	0.2087E-02	0.4960E-04	101748
kusslb.yz165.1gsa	15	16	0.2070E-02	0.4982E-04	101748
kusslb.yz166.1gsa	15	16	0.2052E-02	0.5002E-04	101748
kusslb.yz167.1gsa	15	16	0.2032E-02	0.5022E-04	101748
kusslb.yz168.1gsa	15	16	0.2010E-02	0.5042E-04	101748
kusslb.yz169.1gsa	15	16	0.1985E-02	0.5062E-04	101748
kusslb.yz170.1gsa	15	16	0.1958E-02	0.5082E-04	101748
kusslb.yz171.1gsa	15	16	0.1928E-02	0.5103E-04	101748
kusslb.yz172.1gsa	15	16	0.1895E-02	0.5125E-04	101748
kusslb.yz173.1gsa	15	16	0.1858E-02	0.5149E-04	101748
kusslb.yz174.1gsa	15	16	0.1819E-02	0.5178E-04	101748
kusslb.yz175.1gsa	15	16	0.1776E-02	0.5213E-04	101748
kusslb.yz176.1gsa	15	16	0.1730E-02	0.5259E-04	101748
kusslb.yz177.1gsa	291	381	0.1737E-02	0.5320E-04	101748
kusslb.yz178.1gsa	291	381	0.1740E-02	0.5399E-04	101748
kusslb.yz179.1gsa	291	381	0.1739E-02	0.5502E-04	101748
kusslb.yz180.1gsa	291	381	0.1733E-02	0.5629E-04	101748
kusslb.yz181.1gsa	291	381	0.1721E-02	0.5783E-04	101748
kusslb.yz182.1gsa	291	381	0.1702E-02	0.5964E-04	101748
kusslb.yz183.1gsa	291	381	0.1675E-02	0.6169E-04	101748
kusslb.yz184.1gsa	291	381	0.1640E-02	0.6396E-04	101748
kusslb.yz185.1gsa	291	381	0.1597E-02	0.6640E-04	101748
kusslb.yz186.1gsa	291	381	0.1544E-02	0.6896E-04	101748
kusslb.yz187.1gsa	289	380	0.1484E-02	0.7159E-04	101748
kusslb.yz188.1gsa	289	380	0.1421E-02	0.7426E-04	101748
kusslb.yz189.1gsa	289	380	0.1350E-02	0.7692E-04	101748
kusslb.yz190.1gsa	289	380	0.1272E-02	0.7957E-04	101748
kusslb.yz191.1gsa	289	380	0.1190E-02	0.8222E-04	101748
kusslb.yz192.1gsa	289	380	0.1105E-02	0.8490E-04	101748
kusslb.yz193.1gsa	289	380	0.1022E-02	0.8772E-04	101748
kusslb.yz194.1gsa	289	380	0.9405E-03	0.9078E-04	101748
kusslb.yz195.1gsa	290	381	0.9405E-03	0.9403E-04	101748
kusslb.yz196.1gsa	292	381	0.9269E-03	0.9581E-04	101748
kusslb.yz197.1gsa	291	381	0.8194E-03	0.9558E-04	101748
kusslb.yz198.1gsa	289	380	0.7573E-03	0.9542E-04	101748
kusslb.yz199.1gsa	290	381	0.7573E-03	0.9670E-04	101748
kusslb.yz200.1gsa	84	381	0.7307E-03	0.9856E-04	101747

Location and values for peak and average SAR for total volume of exposed tissue

kusslb.yz52.1gsar	229	141	0.5958E+00	0.4893E-02	15160451

10 Conclusions

The FDTD method was used to calculate the far field antenna patterns and near electric and magnetic fields for the AT&T RU antenna radiating in free space for an input power of 79.62 mW split evenly between two coaxial antenna input feeds. The antenna patterns and gain closely agreed with the antenna manufacturer's measured values. The calculated near electric and magnetic fields were below the FCC MPL and closely agreed with measurements made in the SPEAG laboratory in Zurich at all locations where measured outside of the radome. The measurements of the electric fields made by SARTest laboratory in London were all below the FCC MPL and agreed with the calculations at all locations except at the radome. At the surface of the radome the SARTest measured electric field strengths ranged from a high of 72.4 V/m to a low of 68.5 V/m (0.95 to 1.4 dB above the FCC MPL). The specified accuracy of the SARTest measurement system was +/- 2 dB. The respective calculated maximum E-field and H-field strengths at the surface of the radome were 0.85 dB and 2.4 dB below the FCC MPL.

Table 10.1 Summary and Comparison of Calculated and Measured Maximum SARs to FCC MPL for Various Tissue Models Exposed to AT&T RU Antenna.

Model	Peak SAR (W/kg)		1Gram Avg. SAR (W/kg)		dB from FCC MPL	
	FDTD	Meas.	FDTD	Meas.	e.i.r.p.=2.54 W	e.i.r.p.=2.0 W
SPEAG Head, nose over array	0.194	0.081	0.132	-	-10.8	-11.9
SPEAG Head, nose over patch	3.49	1.29	1.53	-	-0.194	-1.23
SPEAG Generic Phantom, side over patch	-	0.717	-	0.432	-5.69	-6.73
REMCOM Head, nose over array	0.439	0.20*	0.0686	-	-13.7	-14.7
Inhomogeneous Slab (2 feeds)	0.805	-	0.346	-	-6.65	-7.69
Inhomogeneous Slab (1 feed)	0.849	-	0.363	-	-6.44	-7.48
Homogeneous Slab	0.890	0.860	0.596	0.484	-5.19	-6.23

* SARTest head with layer of skin

Peak and 1 gram average SARs for various computer tissue phantoms consisting of homogeneous and inhomogeneous human head and planar torso models exposed to the AT&T RU antenna were calculated. The calculations agreed very well with measurements made on exposed equivalent physical phantoms in the SPEAG laboratory.

The measurements of SAR by the SARTest laboratory were no greater generally much lower than the calculated values. In general it is expected that measured values of SAR in the exposed phantoms will be below the peak-calculated values since the latter cover the entire phantom and have high spatial resolution (1-mm). On-the-other-hand for the former the resolution and accessibility of tissues near the boundaries of the model is dictated by the size of the measurement probe. Test calculations were made of the peak and 1 gram average SARs in a inhomogeneous slab torso model exposed to the AT&T RU antenna with the full 79.62 mW of power feed to a single (bottom) feed. The calculated SARs were within 0.23 dB from the values obtained from the same model exposed to the antenna with the input power split between evenly between the feeds. Since the SAR distributions in slab model exposed against the radome are closely related to the adjacent near field distribution it can be concluded that the near field distribution for the single feed antenna is nearly identical with that for the double feed antenna. Thus it follows that the maximum SARs calculated for all other models exposed the double feed antenna would be similar to those calculated for exposure to the single feed antenna.

The maximum peak and 1 gram average SAR calculations and measurements for all tested models are summarized and compared to the FCC MPL in Table 10.1. All of the obtained SARs were below the FCC MPL. The comparisons to the FCC MPL are made both for an antenna e.i.r.p. of 2.54 watts which was the basis of the calculations and an antenna e.i.r.p. of 2.0 watts which is expected to that used for the operational antenna. Dashes indicate exposure scenarios where measurements were not made. Since measurements could not be made in a number of places where maximum SARs were calculated, the locations of maximum measured SARs don't necessarily correspond to the same locations of maximum calculated SARs and can be significantly lower. The results in Table 10.1 show that the worst case scenario is exposure of the head with the nose in contact with the radome and centered over the patch producing the highest fields, resulting in an exposure of 1.23 dB below the FCC MPL. It is highly unlikely that such an exposure would last for the 30 minute averaging time specified by the FCC and most likely would only be momentary if it ever occurred in practice. For example an 18-second exposure under these conditions would result SARs more than 21 dB below the FCC MPL. The table indicates that exposures with the side of the head or torso (slab models) against the radome would be more than 6.23 dB below the FCC MPL. As expected the exposure of the more life-like inhomogeneous head model results in SARs lower than obtained from the worst case homogeneous models.

11 References

ANSI/IEEE (1992): "IEEE Standard for Safety Levels with Respect to Human Exposure to Radio Frequency Electromagnetic Fields, 3 kHz to 300 GHz." ANSI/IEEE C95.1-1992, New York, NY; IEEE.

Federal Communications Commission (1996): “FCC Report and Order in ET Docket 93-62, 61 Federal Register 41006”, Technical Report, Federal Communications Commission, Office of Engineering and Technology, Washington, D.C., August 1996.

Gabriel C (1996): “Compilation of the Dielectric Properties of Body Tissues at RF and Microwave Frequencies.” Final Technical Report AL/OE-TR-1996-0037, June, Armstrong Laboratory, Brooks Air Force Base, Texas 78235-5102. (See Internet URL www.fcc.gov/fcc-bin/dielec.sh)

Gandhi OP, Lazzi G, Furse CM (1996): Electromagnetic absorption in the human head and neck for mobile telephones at 835 and 1900 MHz. IEEE Trans Microwave Theory Tech MTT-44:1884-1897.

Ho HS, Guy AW (1975): Development of dosimetry for RF and microwave radiation - II: Calculations of absorbed dose distributions in two sizes of muscle-equivalent spheres. Health Physics 29:317-324.

Lau, R. W., Sheppard, G., Howard, G., and Blechen, N. M. (1986): “The modeling of biological systems in three dimensions using the time-domain- finite-difference method: I. The implementation of the model; II. The application and experimental evaluation of the method in hyperthermia applicator design,” Phys. Med. Biology, vol. 31, pp. 1247-1266.

Liao ZP, Wong HL, Yang GP, Yuan YF (1984): A transmitting boundary for transient wave analysis. Scientia Sinica 28:1063-1076.

Rosen R. and Vander Vorst A., Guest Editors, (1996), “Part II of two parts: Special issue on medical applications and biological effects of RF/Microwaves,” MTT-44:1755-1973.

Sullivan D.M., Borup D.T. and Gandhi O.P. (1987), “Use of the finite difference time domain method in calculating absorption in human tissues,” IEEE Trans. Bioemed. Eng., BME-34:148-157.

Sullivan D.M., Gandhi O.P. and Taflove A. (1988), “Use of the finite difference time domain method in calculating EM absorption in man models,” IEEE Trans Microwave Theory and Tech., BME-35:179-185.

Taflove, A, and Brodwin, M. E. (1975a), “Numerical solution of steady-state electromagnetic scattering problems using the time-dependent Maxwell’s equations,” IEEE Trans. Microwave Theory Tech.. vol. 23, pp. 623-630.

Taflove, A, and Brodwin, M. E. (1975b), “Computation of the electromagnetic fields and induced temperatures within a model of the microwave-irradiated human eye,” IEEE Trans. Microwave Theory Tech.. vol. 23, pp. 888-896.

Taflove, A. (1980), “Application of the finite difference time domain method to sinusoidal steady state electromagnetic penetration problems,” IEEE Trans. Electromagnetic Compatibility, EMC-22:191-202.

Taflove, A. (1988), “Review of the formulation and applications of the finite difference time domain method for numerical modeling of electromagnetic wave interactions with arbitrary structures. Wave Motion,” 10-6:547-583.

Yee, K. S. (1966): “Numerical solution of initial boundary value problems involving Maxwell’s equations in isotropic media,” IEEE Trans. Antennas and Propagation, vol. 14, pp. 302-307.